Received: 12 March 2026 | Revised: 25 May 2026 | Accepted: 16 June 2026 | Published online: 1 July 2026

RESEARCH ARTICLE

Smart Wearable Technology
2026, Vol. 00(00) 1–12
DOI: 10.47852/bonviewSWT62029603

BON VIEW PUBLISHING

A Modular Closed-Loop Wearable Platform for Sweat Extraction, Analysis, and Drug Delivery

Jinhang Ma[1], Shuo Yang[2], Sijie Yin[1,*], Xiaohan Wang[3,*] and Ningning Song[2,*]

[1] *School of Automation, Beijing Institute of Technology, China*

[2] *School of Materials Science & Engineering, Beijing Institute of Technology, China*

[3] *Institute of Spacecraft System Engineering, China Academy of Space Technology, China*

Abstract: Precision medicine requires wearable systems capable of transforming real-time physiological sensing into adaptive therapeutic intervention. However, existing sweat-based platforms remain fragmented, typically focusing on sensing alone and relying on empirical threshold-triggered control strategies. Here we report a modular, model-driven wearable architecture that integrates active sweat extraction, multi-channel electrochemical sensing, and ion-electroosmotic transdermal drug delivery within a unified closed-loop framework. Active iontophoretic sweat extraction enables stable sampling under non-exertional conditions, while standardized multi-channel electrochemical interfaces support flexible biomarker configuration on a shared hardware backbone. Beyond hardware integration, we introduce a dual-layer control architecture combining data-driven physiological prediction with a physics-informed iontophoretic transport model, establishing a quantitative and interpretable mapping from sensed biomarkers to calibrated dosing decisions. Experimental results demonstrate accurate multi-biomarker sensing performance, including glucose sensing linearity (R^2 = 0.9913) and ascorbic acid sensing linearity (R^2 = 0.9965), together with near-linear controllability of transdermal delivery (R^2 > 0.99), consistent with the proposed transport model. By introducing a model-based quantitative regulation framework beyond conventional threshold-triggered actuation, this work provides a generalized system architecture and methodological foundation for precision and personalized wearable therapeutics.

Keywords: wearable closed-loop systems, sweat sensing, iontophoretic drug delivery, model-driven control

1. Introduction

Precision and personalized medicine demand wearable systems that extend beyond passive monitoring toward integrated therapeutic functionality. Rather than merely sensing physiological states, next-generation devices must transform real-time physiological information into timely, individualized interventions. Within this context, wearable platforms integrating biochemical sensing, computational decision-making, and therapeutic actuation have emerged as an important direction toward closed-loop personalized healthcare systems [1–4]. Despite substantial advances in wearable biosensing, however, most existing systems remain functionally incomplete from a systems-level perspective.

Sweat has attracted increasing attention as a noninvasive biofluid enriched with diverse physiological markers [5–7]. Numerous studies have demonstrated wearable electrochemical sweat sensing, including glucose detection using microfluidic platforms [8], electrochemical metabolite sensing strategies [9], and multiplex biochemical analysis systems [10]. Yet most sweat-based wearables focus exclusively on sensing performance, implicitly assuming continuous sweat availability while overlooking the engineering challenge of reliable sample acquisition. In practice, sweat secretion under sedentary conditions is often insufficient or intermittent. Active sweat induction should therefore be regarded not merely as an auxiliary feature but as a foundational component of wearable sweat-based feedback systems.

At the systems level, current research remains fragmented across sweat sensing, electrically driven transdermal delivery, and integrated validation. While recent studies have explored multifunctional therapeutic wearables [11], sweat sensing with transdermal delivery [3], and model-based closed-loop control strategies [4], fully unified architectures integrating induction, biochemical detection, decision-making, and therapeutic actuation remain limited. Such incomplete integration constrains both robustness and translational potential.

***Corresponding authors:** Sijie Yin, School of Automation, Beijing Institute of Technology, China. Email: yinsijie@bit.edu.cn, Xiaohan Wang, Institute of Spacecraft System Engineering, China Academy of Space Technology, China. Email: wangxiaohan2@cast501.cn and Ningning Song, School of Materials Science & Engineering, Beijing Institute of Technology, China. Email: songningning@bit.edu.cn

Beyond hardware-level fragmentation, a more fundamental limitation lies in the prevailing control paradigm. Existing sweat-based regulation strategies predominantly rely on threshold-triggered actuation, whereby intervention is initiated once a predefined sensor value is exceeded [12]. While straightforward, this approach neglects inter-individual variability, temporal physiological dynamics, and measurement uncertainty. Consequently, the relationship between sensing and intervention lacks theoretical grounding and remains insufficient for precision therapeutics.

Here, we present a modular, extensible, and model-driven wearable platform for sweat-based closed-loop analysis and transdermal intervention. The system integrates active sweat extraction, multi-channel electrochemical sensing, and ion-electroosmotic drug delivery within a unified architecture. By treating acquisition, detection, and actuation as coequal components of a feedback loop, the platform enables continuous operation even under non-exertional conditions. A defining characteristic of the system is its architectural extensibility. Standardized electrical interfaces and modular hardware abstraction decouple application-specific sensor design from the core control circuitry, enabling parallel multimodal sensing and expansion to diverse biomarkers without hardware redesign. The platform thus functions as a generalizable research infrastructure rather than a task-specific device.

More importantly, we introduce a data-informed, mathematically interpretable control framework that replaces empirical threshold triggering. By establishing a quantitative mapping between physiological measurements and dosing decisions, the system transitions from binary activation logic to model-based intervention optimization [4, 13, 14]. Parameterized calibration enables adaptation to inter-individual variability, providing a principled foundation for precision and personalized therapeutics [15, 16]. In summary, this work establishes a generalized system architecture and methodological foundation for sweat-driven feedback regulation. The principal contributions are threefold: (i) the realization of an integrated sweat induction-sensing-actuation architecture at the system level; (ii) a modular multi-channel electrochemical interface supporting diverse sensing modalities; and (iii) a data-driven, interpretable dosing control strategy that enables adaptive and individualized regulation.

2. System Architecture and Design Principle

The proposed system is conceived as a unified closed-loop platform integrating sweat extraction, biochemical sensing, decision computation, and ion-electroosmotic drug delivery. Rather than optimizing individual modules in isolation, the design emphasizes system-level coherence, modularity, and controllability to meet the stability and engineering feasibility requirements of wearable applications in real-world environments. The overall architecture is organized around a physiological feedback loop, within which information flow, control flow, and material flow are explicitly defined and coordinately structured.

2.1. Overall closed-loop framework

A wearable closed-loop physiological regulation system is developed to integrate physiological sensing, data-driven decision-making, and electrically controlled transdermal drug delivery. The overall concept and structural organization of the system are illustrated in Figure 1. The platform consists of three functional layers: the skin interface, the embedded hardware system, and

Figure 1

Overview of the wearable closed-loop physiological regulation system. (a) Illustration of the wearable system in operation, showing on-body sensing, wireless communication with a mobile device, and cloud-assisted physiological prediction and dosing decision. (b) Structural organization of the closed-loop system, including the skin interface, embedded hardware modules, and host-side control layer enabling sensing, decision-making, and transdermal drug delivery

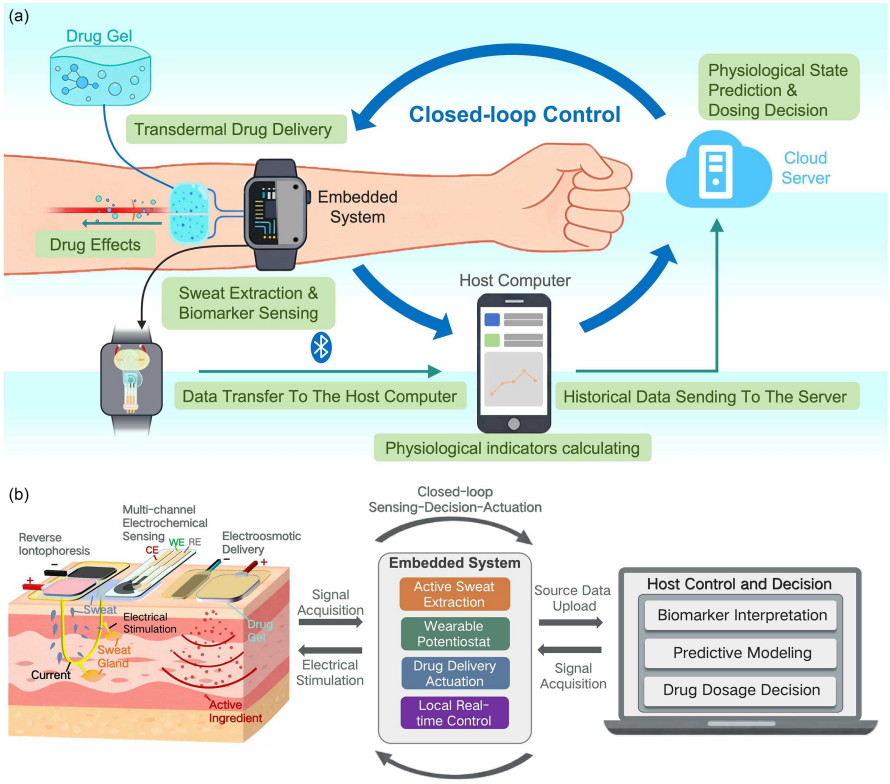

the host-side control application. At the skin interface, reverse iontophoresis is employed to induce sweat extraction under non-exertional conditions, enabling continuous biochemical sampling. The collected sweat is analyzed using a multi-channel electrochemical sensing module that converts biochemical information into electrical signals. These signals are acquired and processed by the embedded system, which integrates key hardware modules including active sweat extraction, wearable potentiostat sensing, drug delivery actuation, and local real-time control, as shown in Figure 1(b). The embedded unit is responsible for signal acquisition and electrical stimulation control while maintaining safe and stable operation. Acquired physiological data are transmitted wirelessly to a host-side application for higher-level analysis and decision-making. At this stage, biomarker interpretation and predictive modeling are performed to estimate physiological states and determine appropriate drug dosage commands. The computed control parameters are subsequently transmitted back to the wearable device to trigger iontophoretic transdermal drug delivery through the drug-loaded hydrogel layer. Through this coordinated process of sensing, computation, and actuation, the system forms a perception–prediction–decision–actuation feedback loop capable of continuous physiological regulation.

2.2. Modular hardware architecture and standardized interfaces

To enable extensibility and compatibility across diverse sensing and intervention tasks, a modular hardware architecture based on standardized functional interfaces is adopted. The core concept integrates sweat extraction, electrochemical detection, and drug delivery onto a unified control mainboard while achieving functional decoupling through clearly defined electrical interfaces. As shown in Figure 2(a), individual functional channels are electrically and logically independent. This interface-level abstraction separates application-specific designs from the core hardware platform, enabling system reconfiguration without

Figure 2

Modular hardware architecture and standardized electrode interfaces. (a) Block diagram of the modular hardware architecture, illustrating functional modules and inter-module communication protocols. (b) Electrode configuration and interface design of the iontophoretic sweat induction module. (c) Electrode configuration compatible with a three-electrode electrochemical sensing system. (d) Electrode configuration and interface design of the iontophoretic transdermal drug delivery module

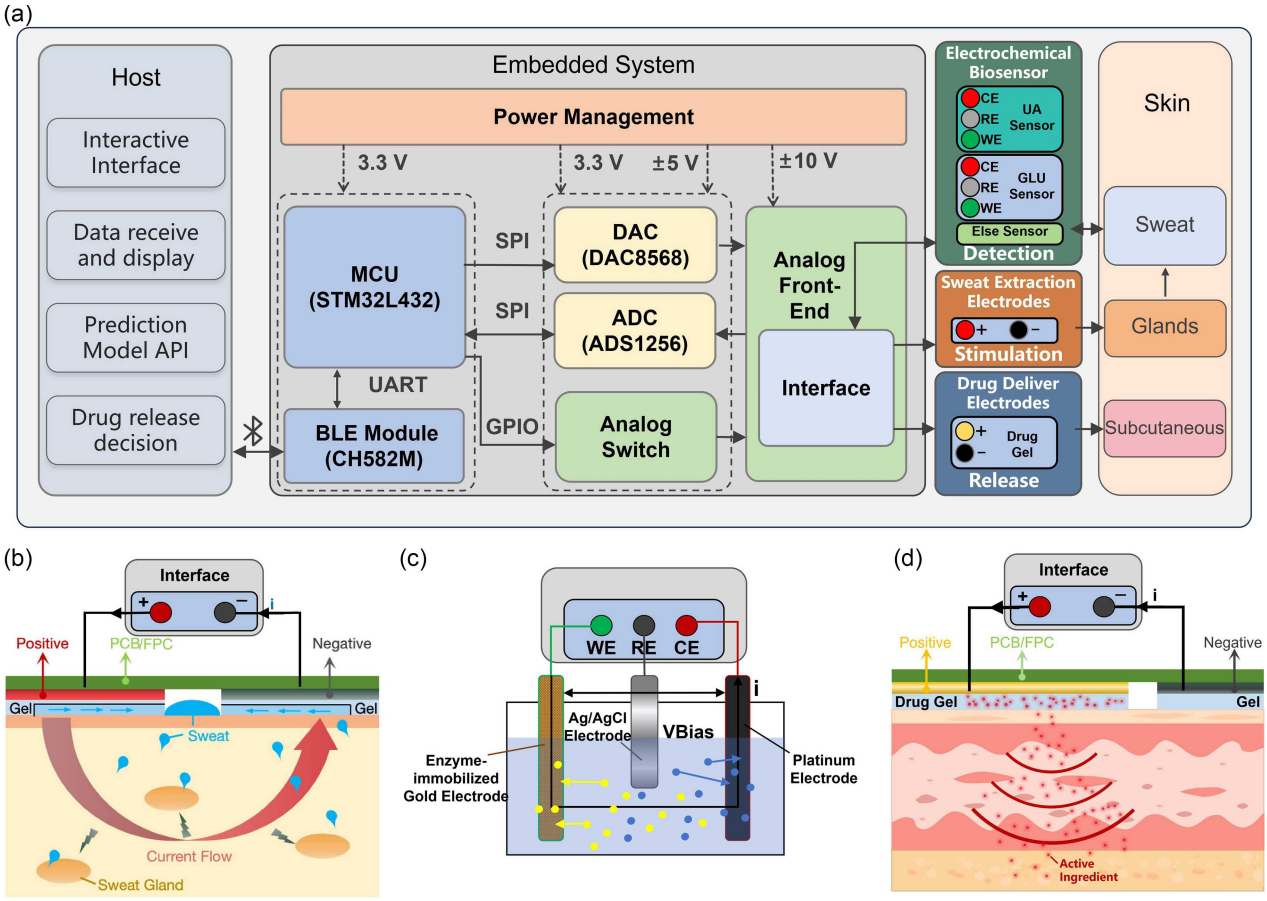

redesigning the mainboard and supporting scalable deployment across different biomarkers and therapeutic modalities. The sweat induction module adopts an independent two-electrode interface (Figure 2(b)), with designated positive and negative terminals provided by the mainboard. The electrochemical sensing channel employs a standardized three-electrode interface—working electrode (WE), reference electrode (RE), and counter electrode (CE)—as shown in Figure 2(c). The mainboard specifies only the electrical connection scheme without constraining electrode materials or geometries, allowing flexible integration of diverse electrochemical sensors and parallel implementation of multiple detection mechanisms. Electrode structure and materials can be optimized or replaced according to sweat induction efficiency and user comfort requirements. Similarly, the transdermal drug delivery module employs an independent two-electrode interface (Figure 2(d)). The mainboard reserves positive and negative terminals, while the drug reservoir, electrode configuration, and functional materials remain externally definable to accommodate specific therapeutic needs.

2.3. Hierarchical control strategy and host–MCU architecture

A hierarchical control strategy is implemented to separate real-time execution tasks from high-level decision computation through a host-microcontroller unit (MCU) architecture. Time-sensitive operations are executed locally on the MCU, whereas computationally intensive prediction and optimization tasks are performed on the host system. At the MCU level, constant-current control, electrochemical signal acquisition, safety monitoring, and execution control operate with millisecond-level responsiveness, ensuring deterministic performance under variations in skin impedance, electrode conditions, or environmental disturbances. At the host level, advanced functions—including physiological state prediction, control strategy computation, and parameter adaptation—are performed. Through wireless communication with the wearable hardware, the host enables real-time monitoring, strategy updating, and system management. This architecture allows complex control algorithms to be incorporated without substantially increasing computational burden, power consumption, or hardware complexity on the wearable device. By decoupling low-level execution from high-level computation, the hierarchical strategy preserves engineering feasibility while maintaining substantial algorithmic scalability.

2.4. Model-driven control architecture

The proposed closed-loop system is built upon a dual-layer, model-driven architecture designed to overcome the limitations of conventional threshold-based control. This framework establishes a transparent and quantitatively grounded pathway from physiological perception to calibrated intervention, enabling individualized therapeutic adaptation. At the prediction and decision layer, physiological forecasting and context-aware strategies replace simple threshold triggering. Predictive models trained on historical data (e.g., short-term glucose trend estimation), together with real-time measurements, are used to estimate near-future physiological states. Based on these estimates, the decision module integrates real-time biomarker concentration, forecast results, safety constraints, and system states (e.g., post-delivery intervals) to generate a quantified therapeutic demand. This formulation transforms control logic from binary threshold responses into a dose optimization problem. At the execution layer, the quantified demand is translated into precise hardware commands via a physics-informed feedforward model of iontophoretic transport. The control-oriented model establishes a deterministic and interpretable mapping between controllable electrical parameters (current i and duration t) and delivered drug amount (M), approximated as:

$$\mathrm{M} \approx K \cdot i \cdot t \tag{2–1}$$

where K encapsulates skin electrophysiological properties and formulation-specific characteristics. Individualized parameter calibration is supported to account for inter-subject variability. By integrating data-driven prediction models, multi-factor decision strategies, and physics-based execution modeling, the proposed framework forms a coherent and interpretable perception–prediction–decision–actuation loop, providing a methodological foundation for personalized and precision adaptive therapy.

3. Module Implementation and Experimental Methods

3.1. Active sweat induction module

The active sweat induction module is designed to enable controlled and localized stimulation of sweat secretion on the skin surface, thereby eliminating reliance on spontaneous perspiration. Sweat induction is based on reverse iontophoresis, in which low-intensity electrical current drives directional ionic migration across the skin barrier, accompanied by electroosmotic solvent flow that transports sweat constituents toward the skin surface. To accommodate inter-individual variability and temporal fluctuations in skin condition, the module employs a constant-current stimulation strategy combined with real-time skin impedance feedback. By targeting the effective current density applied to the skin, the system compensates for impedance variations arising from hydration state, temperature changes, or electrode contact conditions. The measured impedance signal is used to dynamically adjust the driving voltage, ensuring stable maintenance of the preset current output. Safety considerations are integrated at both hardware and software levels. The stimulation current density and duration are constrained within established dermatological safety limits. Hardware-level current-limiting mechanisms are implemented alongside software-defined parameter boundaries. Upon detection of either a relative impedance increase exceeding 50% of the baseline value measured at stimulation onset or an absolute impedance exceeding 200 kΩ, stimulation is automatically terminated.

3.2. Electrochemical sensing module

The electrochemical sensing module adopts a multi-channel parallel architecture, with each channel configured as a standard three-electrode system comprising a WE, RE, and CE. Electrical connections and signal processing pathways are independently implemented for each channel, enabling simultaneous detection of multiple biomarkers while minimizing inter-channel interference. Each channel can be configured with distinct measurement protocols, allowing concurrent execution of different electrochemical techniques within the same operational cycle. The selection of detection techniques is determined by the electrochemical characteristics of the target analyte and corresponding electrode functionalization strategies. Beyond the specific

demonstrations presented herein, the sensing module is designed as a general-purpose, multi-technology-compatible platform. The system supports up to 12 commonly used electrochemical techniques, including chronoamperometry (*i–t*), differential pulse voltammetry (DPV), cyclic voltammetry, and related pulse-based methods [17]. A complete list of supported techniques is provided in the Supplementary Information (T1). The analog front-end and potentiostat control circuitry incorporate a wide compliance voltage (±10 V) to accommodate high solution resistance and significant iR drop commonly encountered in sweat sensing under dynamic secretion conditions. This wide-voltage design maintains stable electrode potential control despite substantial interface impedance variations, thereby enhancing measurement robustness in wearable applications.

3.3. Drug delivery module

The drug delivery module operates based on iontophoretic transdermal transport [18]. Under an applied electric field, solvent flow within the skin is induced, carrying dissolved therapeutic agents across the skin barrier into the underlying tissue. This mechanism obviates the need for mechanical pumps or complex microfluidic structures, facilitating integration within wearable systems. A constant-current closed-loop control strategy regulates the delivery process. Real-time current feedback compensates for dynamic variations in skin impedance, maintaining stable electroosmotic driving conditions. Consequently, delivered dosage can be quantitatively modulated via electrical stimulation parameters rather than relying on passive diffusion assumptions. The module is architecturally aligned with the system-level control model. Electrical stimulation parameters generated by the control algorithm are directly mapped onto the iontophoretic transport process, establishing a clear and interpretable correspondence between physiological state estimation and physical actuation.

To establish a quantitative relationship between applied electrical parameters and delivered drug dosage, a control-oriented iontophoretic transport model is introduced. Although transdermal iontophoresis theoretically involves electromigration, electroosmosis, and passive diffusion, a simplified formulation is adopted to ensure computational efficiency on embedded platforms. For many therapeutic agents of interest, such as peptides or near-neutral macromolecules, electromigration contributions are negligible; thus, electroosmotic flow is treated as the dominant transport mechanism. The electroosmotic velocity ueo can be approximated by the Helmholtz–Smoluchowski relation:

$$u_{eo} \approx \frac{\varepsilon\zeta}{\eta\sigma}\,\mathrm{E} \tag{3–1}$$

where ε is the dielectric constant, ζ the interfacial zeta potential, η the solvent viscosity, and E the applied electric field strength. Considering the relation $E \approx i/\sigma$, where i denotes current density and σ the effective skin conductivity, the neutral drug mass flux per unit area J can be approximated as:

$$\mathrm{J} \approx C_{eff} \cdot \frac{\varepsilon\zeta}{\eta\sigma} \cdot i \tag{3–2}$$

where C_{eff} is the effective drug concentration within the reservoir. Integrating over delivery area A and stimulation duration t yields the cumulative delivered amount:

$$\mathrm{M} \approx \mathrm{K} \cdot i \cdot t$$

with

$$\mathrm{K} = \mathrm{A} \cdot \mathrm{Ceff} \cdot \frac{\varepsilon\zeta}{\eta\sigma} \tag{3–3}$$

representing a lumped system parameter incorporating formulation and skin properties. Under the short stimulation durations investigated here, K is not expected to vary substantially. The dominant short-term variability is likely associated with changes in skin–electrode interfacial impedance related to hydration state and contact quality. The constant-current strategy can partially mitigate their influence on delivery stability. This linearized formulation provides a physically interpretable mapping from controllable electrical parameters to delivered dose within the closed-loop framework.

3.4. Data-driven prediction and decision model

The decision layer relies on a data-driven physiological prediction model implemented as an independent host-side software module. Glucose regulation is used as a representative case. The model, trained on the publicly available OhioT1DM time-series dataset [19], employs supervised random forest regression to predict glucose trends 30 min ahead based on historical glucose values, insulin administration records, and carbohydrate intake. The validated model outputs quantitative short-term physiological forecasts. The decision engine operates as a rule-based multi-factor strategy module. Inputs include real-time sensor data, predicted trends, historical dosing records (enforcing minimum dosing intervals), and predefined safety constraints such as hypoglycemia thresholds. Rather than relying on single-value threshold triggering, the strategy evaluates predicted slope, deviation from target range, and safety boundaries to compute a quantified dosing target. Each decision is accompanied by a structured rationale tag (e.g., "predicted upward trend exceeding range") to enhance interpretability. This framework transforms empirical threshold-based control into a computable decision process jointly driven by data and formalized rules, forming the software foundation for personalized and precision regulation.

3.5. Software architecture and data flow

A layered software architecture coordinates sweat induction, sensing, and drug delivery modules. Low-level firmware on the embedded controller manages real-time tasks, including signal acquisition, closed-loop current regulation, and safety monitoring, whereas high-level instruction scheduling, data synchronization, and state management are executed through structured command streams. System operation follows a finite-state machine model, with distinct states corresponding to sweat induction, sensing, delivery, idle, and fault conditions. State transitions are governed by timing constraints, sensor feedback, and safety criteria, ensuring deterministic and reliable continuous operation. All data streams are timestamped using a unified reference to support subsequent closed-loop control and analysis. A standardized data pipeline connects sensing and actuation. The MCU packages real-time physiological measurements and relevant system states for transmission to the host. The host invokes prediction and decision modules to compute a target dose and associated rationale and then transmits instructions back to the MCU. Based on the dosing control model, the MCU resolves specific stimulation parameters and executes delivery. This bidirectional flow completes automated

Figure 3

Host-side application interface enabling closed-loop regulation and system supervision. (a) Real-time glucose measurements and short-term model-based predictions displayed in a unified time-series view. (b) Structured dosing decision prompt triggered upon satisfaction of control criteria, together with the corresponding dosing execution progress display. (c) Statistical summary of recent glucose dynamics. (d) Historical log of dosing events and meal records for intervention traceability. (e) Device connectivity status, sensing configuration parameters, and supervised manual inputs for dosing and meal annotation

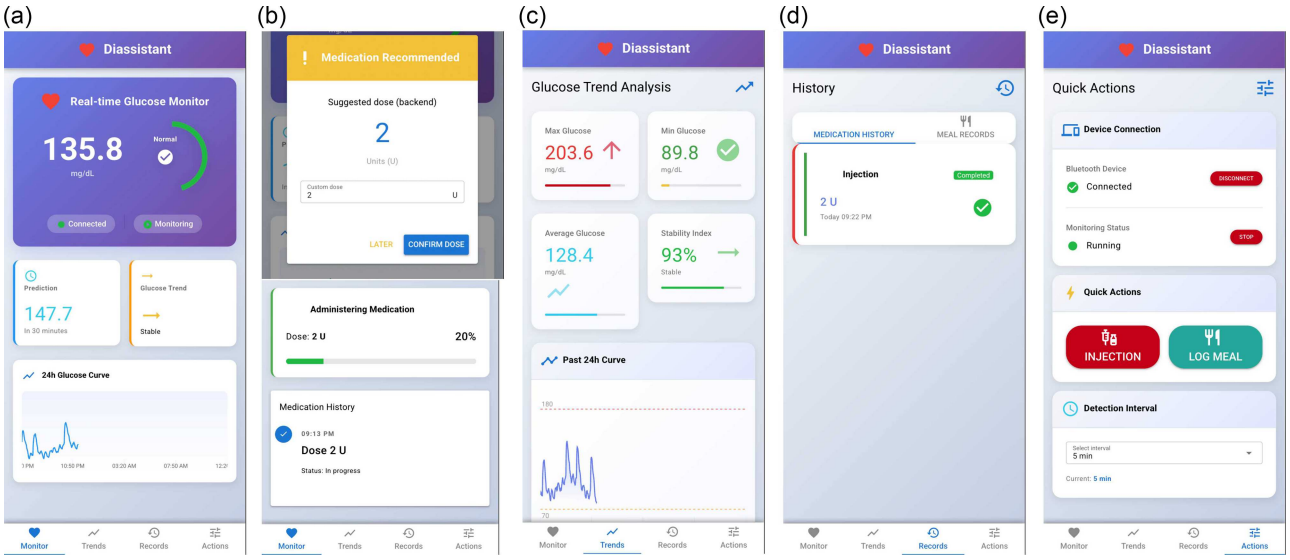

perception–prediction–decision–actuation integration. To facilitate real-time visualization and user-supervised interaction, a host-side application was developed to integrate physiological monitoring, predictive analysis, and dosing execution within a unified interface. The application displays real-time glucose measurements alongside 30-minute-ahead predictions, provides structured decision prompts when dosing criteria are satisfied, and logs all actuation events and contextual inputs (e.g., meal records) for traceability. Representative interface screenshots are shown in Figure 3, illustrating the operational realization of the perception–prediction–decision–actuation workflow.

4. Experimental Results and Closed-Loop Validation

4.1. Sweat extraction performance

To evaluate the effectiveness of the iontophoretic induction module, a dedicated experimental setup was constructed to quantify localized sweat accumulation on the skin surface. The induction interface consisted of a gold electrode patterned on a flexible printed circuit substrate and covered with a hydrogel layer that served both as an electrolyte medium and as a soft skin contact interface. A Polydimethylsiloxane (PDMS) holder was used to stabilize the hydrogel layer and reduce the interfacial impedance between the electrode and the skin. The entire structure was mechanically secured using a custom 3D-printed fixture to maintain stable contact during the experiment. The assembled device was positioned on the thumb of the participating authors, where electrical stimulation was applied to induce localized sweat secretion (Figure 4(a)–(e). Sweat accumulation was quantified indirectly by monitoring the change in skin surface humidity beneath the sensing interface. Measurements were recorded at multiple time points over a 20 min stimulation period, and three independent experiments were conducted. The experimental group received iontophoretic stimulation, whereas the control group was monitored under identical conditions without electrical induction. As shown in Figure 4(f), the skin surface humidity of the experimental group increased progressively during stimulation, while the control group remained nearly constant. After approximately 15 min, a clear separation between the two groups became evident, indicating the onset of significant sweat secretion induced by the electrical stimulation. When the difference between experimental and control measurements was analyzed across replicates (n = 3), the increase in sweat-related humidity became pronounced and remained stable after 15 min (Figure 4(g)). These results demonstrate that the proposed induction module can reliably generate localized sweat under resting conditions, thereby providing a stable sample source for downstream electrochemical sensing.

4.2. Electrochemical sensing performance

The electrochemical sensing front-end exhibits a wide dynamic range, supporting current detection up to ±20 mA with a resolution of 100 nA. A compliance voltage of ±10 V accommodates high-impedance systems, while each channel supports independent sampling rates up to 300 Hz. Three channels can operate synchronously, and 12 electrochemical techniques are selectable via host software. The standard test results for the detection performance of all supported detection technologies are presented in Table A1 of the supplementary document. To validate platform versatility, four representative sweat biomarkers were evaluated using the same hardware system. Glucose detection was performed using chronoamperometry (i–t). The WE consisted of glucose oxidase immobilized on carbon cloth modified with Nafion and carbon nanotubes; a platinum wire and Ag/AgCl electrode served as counter and reference electrodes, respectively [20–22]. At an applied potential of +0.6 V (vs Ag/AgCl), sensor current exhibited linear dependence on glucose concentration within 0–2.5 mM (R^2 = 0.9913; sensitivity 22.343 μA mM^{-1}), as shown in Figure 5(a) and (b). Additional biomarkers—including uric acid, tyrosine, and ascorbic

Figure 4
Experimental validation of iontophoretic sweat extraction. (a) PDMS structure used to stabilize the hydrogel interface and reduce skin–electrode impedance. (b) Gold electrode patterned on a flexible printed circuit (FPC) substrate matching the hydrogel geometry. (c) Custom 3D-printed fixture for mechanical stabilization of the interface assembly. (d) Fully assembled induction interface consisting of hydrogel, PDMS holder, electrode, and fixation structure. (e) Photograph illustrating device placement on the thumb of a human subject during sweat extraction experiments. (f) Time-dependent change in skin surface humidity during iontophoretic stimulation compared with the control condition (mean with min–max range, n = 3). (g) Net increase in sweat-related skin humidity (experimental minus control) over time (mean with min–max range, n = 3)

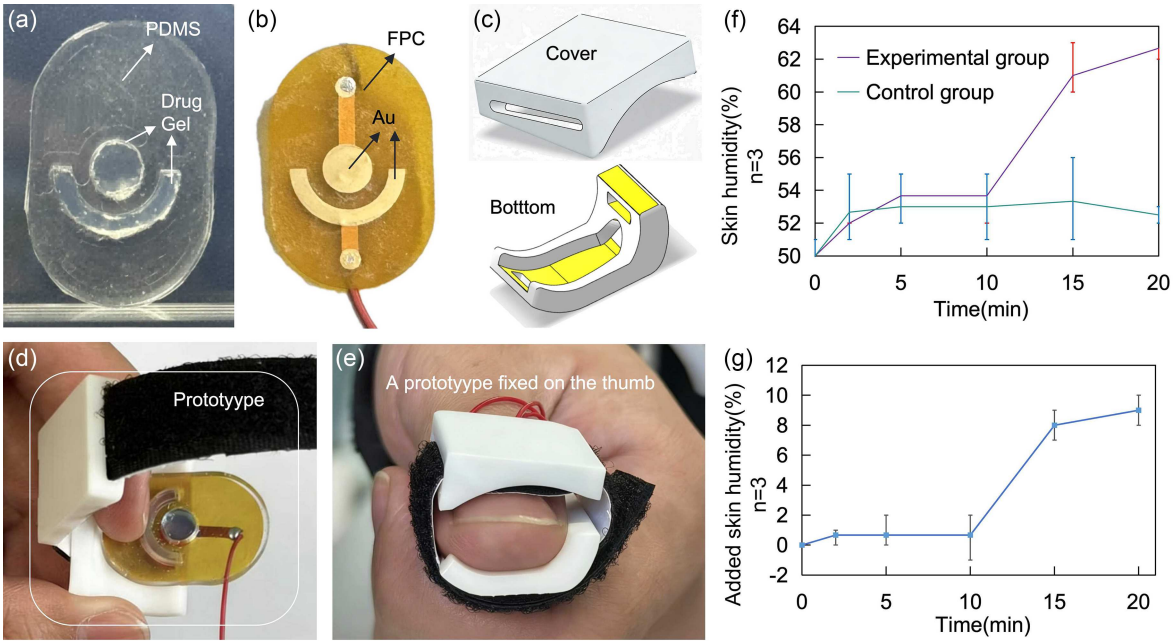

acid—were evaluated to demonstrate compatibility with voltametric and amperometric techniques. Molecularly imprinted polymer-modified carbon cloth served as the WE for uric acid and tyrosine detection using DPV, as shown in Figure 5(c)–(f), revealing characteristic oxidation peaks at approximately +0.32 V and +0.63 V, respectively, with linear responses across tested ranges (uric acid: 0.1–0.5 mM, R^2 = 0.9934; tyrosine: 0–0.2 mM, R^2 = 0.9916). Ascorbic acid detected via i–t at +0.2 V exhibited strong linearity (R^2 = 0.9965; sensitivity 67.06 μA mM^{-1}), as shown in Figure 5(g) and (h). Collectively, these results demonstrate that multiple electrochemical techniques and biomarkers can be realized on the same core circuitry solely through replacement of functionalized WEs, thereby validating the modular and extensible sensing architecture.

4.3. Calibration and validation of the drug delivery model

To experimentally validate the iontophoretic dosing model, an ex vivo porcine skin platform was established using rhodamine B as a model compound (Figure 6(a)–(e)). Fresh porcine skin served as the transport barrier, and a PDMS-based holder was used to stabilize the skin, drug-loaded hydrogel, and flexible gold electrodes during stimulation. Drug penetration depth was quantified by confocal microscopy of cross-sectional skin samples following iontophoretic treatment. Experiments were conducted under varying current densities (0–4 mA cm^{-2}) and stimulation durations of 10, 20, and 30 min. Penetration depths were normalized against passive diffusion controls prior to analysis. As shown in Figure 6(f), penetration depth increased monotonically with current density at a fixed stimulation duration and increased with duration at constant current density. Across the tested parameter space, penetration depth exhibited an approximately linear dependence on the product of current density and stimulation time, with global fitting yielding $R^2 > 0.99$, consistent with the simplified model $M \approx K \cdot i \cdot t$. These results indicate that the proposed linearized iontophoretic model provides a reliable quantitative approximation within the investigated range and is suitable for feedforward dose estimation in closed-loop regulation.

4.4. Performance of the glucose prediction model

To demonstrate model-driven computational feasibility, glucose regulation was implemented as a representative case. The prediction model was trained using the publicly available OhioT1DM dataset and evaluated on its standard independent test set. Model performance was quantified using root mean square error, achieving a best-case value of approximately 17.48 mg dL^{-1} on the test set. This accuracy is comparable to reported wearable glucose prediction studies and sufficient for demonstrating trend-aware closed-loop decision feasibility rather than absolute glycemic correction. Figure 7 presents time-series comparisons between predicted and actual glucose values. The predicted signal closely follows temporal trends with limited phase delay, supporting its applicability within the closed-loop dosing decision framework. No direct physiological mapping between sweat glucose and blood/interstitial glucose is established in the present study. The OhioT1DM dataset was used solely for algorithmic framework validation.

Figure 5

Multi-biomarker electrochemical sensing performance and validation of the iontophoretic transport model. (a) Chronoamperometric (i–t) responses to stepwise increases in glucose concentration from 0 to 2.5 mM. (b) Glucose calibration curve derived from steady-state currents measured at 85 s. (c) Differential pulse voltammetry (DPV) responses for uric acid concentrations ranging from 0 to 0.5 mM. (d) Uric acid calibration curve based on DPV peak currents. (e) DPV responses for tyrosine concentrations from 0 to 0.2 mM. (f) Tyrosine calibration curve derived from DPV peak currents. (g) Chronoamperometric (i–t) responses to ascorbic acid concentrations from 0 to 10 mM. (h) Ascorbic acid calibration curve derived from steady-state currents measured at 35 s

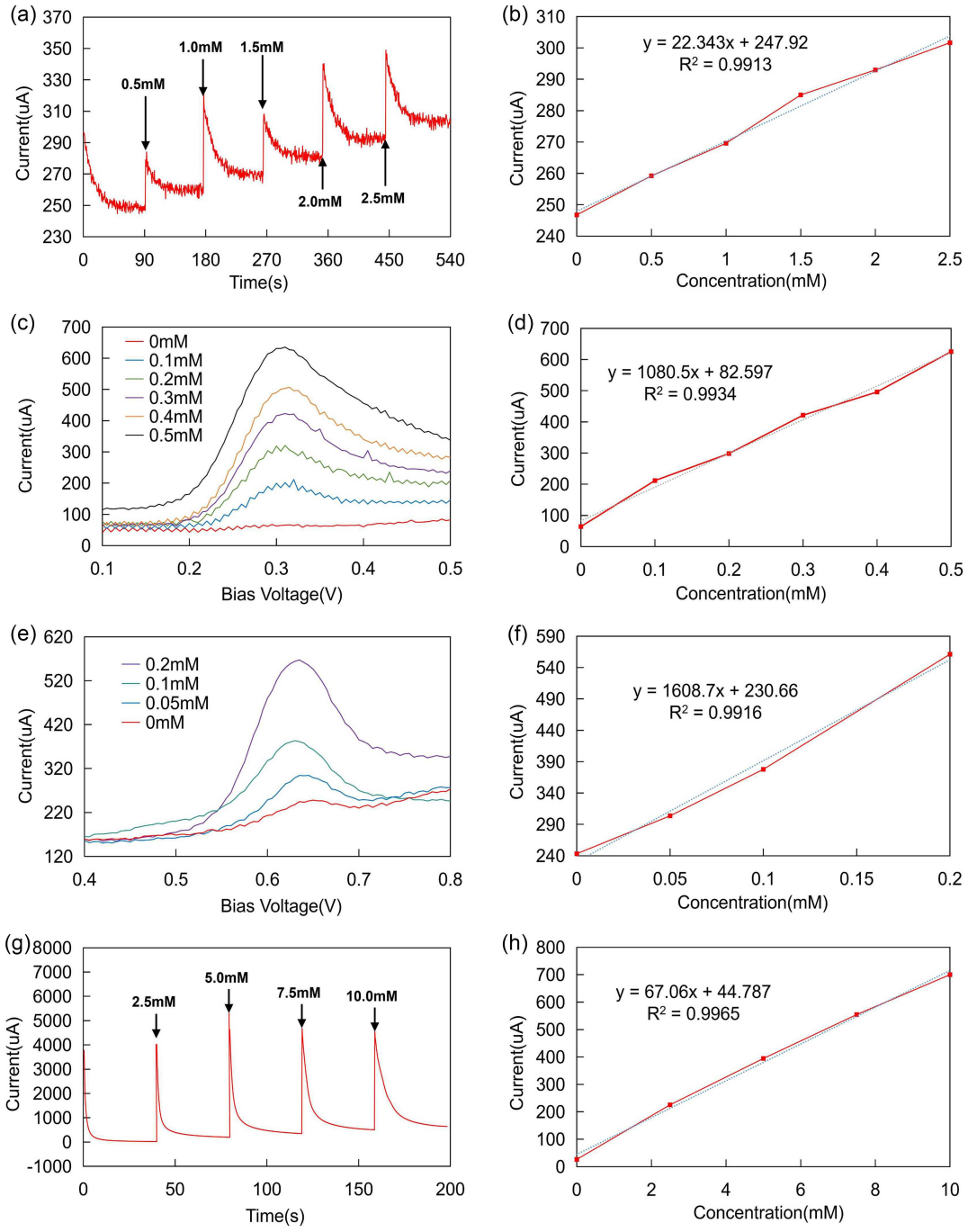

Figure 6

Experimental validation of the iontophoretic drug delivery model using an ex vivo porcine skin platform. (a) Fresh porcine skin used as the ex vivo barrier to simulate human skin. (b) PDMS holder designed to fix the porcine skin, drug-loaded hydrogel, and flexible printed circuit (FPC) gold electrodes during iontophoretic stimulation. (c) Rhodamine B–loaded hydrogel prepared as the model drug formulation. (d) Schematic illustration of the assembled iontophoretic delivery setup integrating porcine skin, hydrogel reservoir, PDMS holder, and electrode interface. (e) Representative cross-sectional samples of treated skin prepared for confocal microscopy to visualize drug penetration. (f) Relationship between drug penetration depth and applied current density at stimulation durations of 10, 20, and 30 min

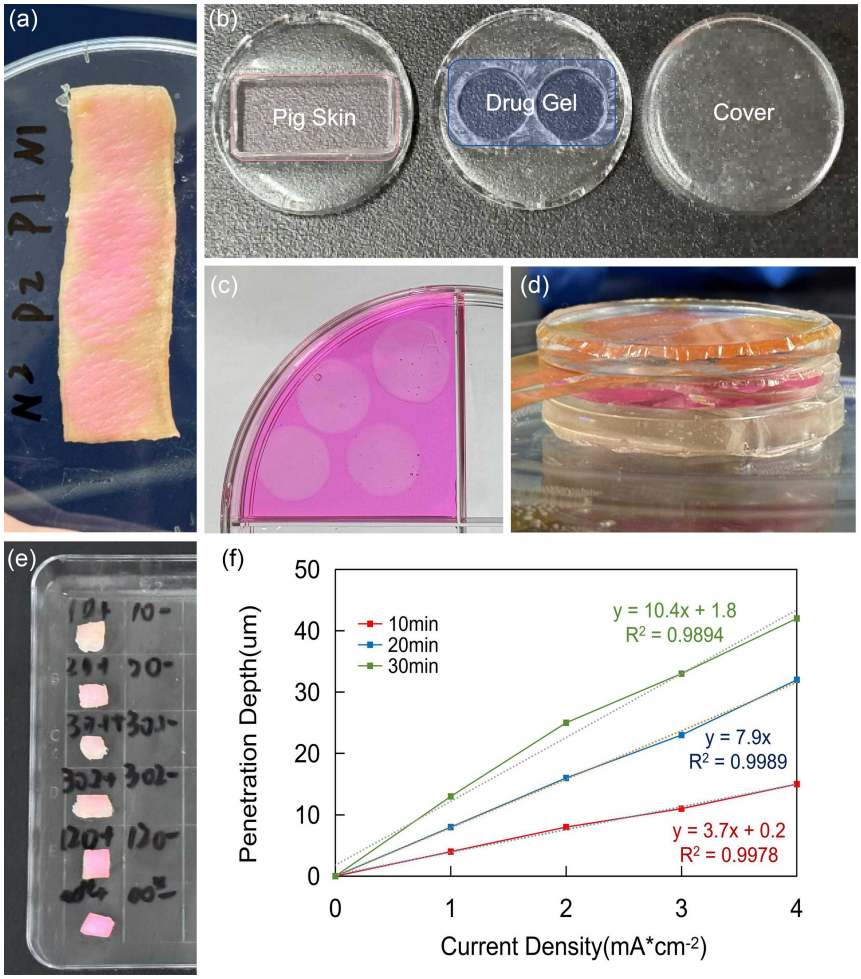

Figure 7

Time-series comparison between predicted and measured glucose levels. Temporal evolution of real-time glucose measurements and corresponding short-term predictions generated by the data-driven physiological model

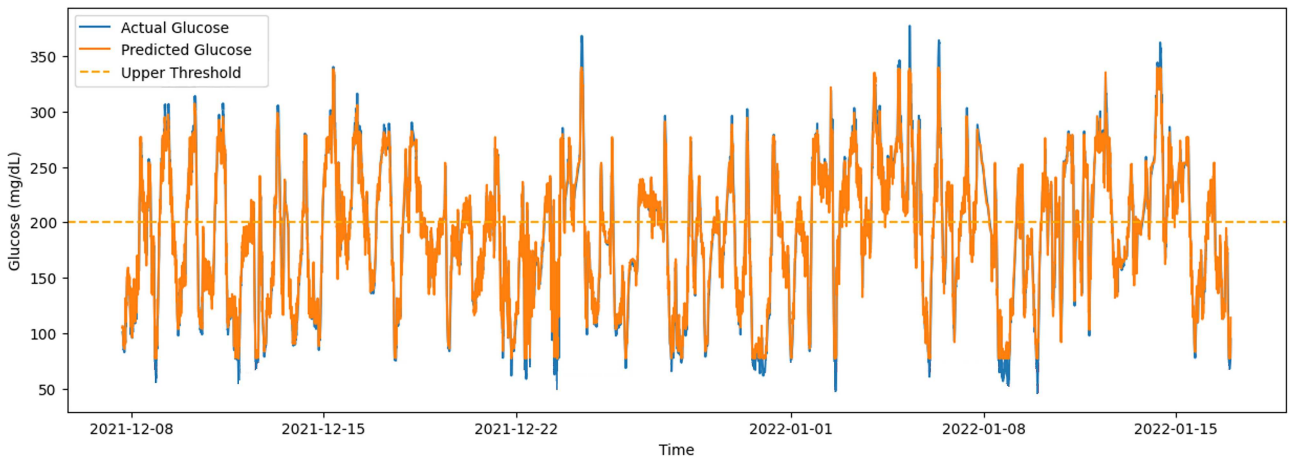

5. Conclusion

This work presents a modular, model-driven wearable platform that integrates active sweat induction, multi-channel electrochemical sensing, and electrically driven transdermal drug delivery within a unified closed-loop regulatory framework. Unlike systems designed for a single biomarker or disease-specific intervention, the proposed architecture emphasizes reconfigurability and hierarchical control abstraction. Through standardized functional interfaces and layered decision strategies, physiological sensing is quantitatively coupled to actuation, enabling a structured perception–prediction–decision–actuation framework at the system level rather than isolated functional modules. Three principal contributions are established at the system level. (1) Active sweat induction is explicitly incorporated into the closed-loop architecture, overcoming the intrinsic limitations of passive sweat collection for continuous and on-demand operation. (2) A modular and extensible multi-channel electrochemical sensing framework is developed, supporting flexible configuration of diverse sensing techniques and biomarkers on a shared hardware backbone. (3) A data-driven and mathematically interpretable control paradigm is introduced, moving beyond threshold-triggered regulation toward model-based quantitative decision-making. This approach enables the incorporation of individual variability and establishes the theoretical foundation for personalized and precision-oriented wearable therapeutics. Several limitations remain. The present study represents an initial system-level feasibility demonstration with a limited sample size and validation primarily under controlled in vitro and ex vivo conditions. The iontophoretic dosing model adopts simplified steady-state assumptions and does not yet account for all dynamic factors encountered in practical wearable operation. In addition, the quantitative coupling between sweat biomarkers and systemic physiological dynamics remains to be formally established. Accordingly, the proposed framework should be regarded as a system-level feasibility demonstration rather than a clinically validated therapeutic platform. Recent studies on self-aligning mechanisms and specialized testbeds further emphasize the importance of robustness and standardized validation in model-driven closed-loop wearable systems [2, 23]. Future work will focus on in vivo animal studies, coordinated multi-loop regulation across multiple biomarkers, and adaptive parameter learning for individualized control. By advancing these directions, the proposed framework may serve as a foundational architecture for next-generation precision medicine and personalized wearable therapeutic systems.

Funding Support

This work is supported by the Natural Science Foundation of Beijing Municipality (2254078, 2262075).

Ethical Statement

The human feasibility experiments described in Section 4.1. Involved only the authors and consisted of low-risk, noninvasive testing conducted within established dermatological safety limits. No patients or external volunteers were involved, and no clinical outcomes or personally identifiable data were collected. All procedures followed the principles of the Declaration of Helsinki, and informed consent was obtained from all participants.

Conflicts of Interest

The authors declare that they have no conflicts of interest to this work.

Data Availability Statement

The source code underpinning the embedded control firmware, host-side application, backend server, and hardware design files is openly accessible in an open-source repository on GitHub (https://github.com/BITMaJinhang/EStat). The repository encompasses firmware source code, PCB schematics, backend implementation, and application interfaces utilized in the present study. All other relevant source data are available from the corresponding authors upon reasonable request.

Author Contribution Statement

Jinhang Ma: Methodology, Software, Validation, Formal analysis, Investigation, Resources, Data curation, Writing – original draft, Writing – review & editing, Visualization. **Shuo Yang:** Data curation. **Sijie Yin:** Conceptualization, Writing – review & editing, Supervision, Project administration, Funding acquisition. **Xiaohan Wang:** Conceptualization, Methodology, Writing – review & editing. **Ningning Song:** Conceptualization, Writing – review & editing, Supervision, Project administration, Funding acquisition.

References

[1] Ates, H. C., Nguyen, P. Q., Gonzalez-Macia, L., Morales-Narváez, E., Güder, F., Collins, J. J., & Dincer, C. (2022). End-to-end design of wearable sensors. *Nature Reviews Materials*, *7*(11), 887–907. https://doi.org/10.1038/s41578-022-00460-x

[2] Brasier, N., Wang, J., Gao, W., Sempionatto, J. R., Dincer, C., Ates, H. C., . . . , & Goldhahn, J. (2024). Applied body-fluid analysis by wearable devices. *Nature*, *636*(8041), 57–68. https://doi.org/10.1038/s41586-024-08249-4

[3] Lee, H., Song, C., Hong, Y. S., Kim, M., Cho, H. R., Kang, T., . . . , & Kim, D.-H. (2017). Wearable/disposable sweat-based glucose monitoring device with multistage transdermal drug delivery module. *Science Advances*, *3*(3), e1601314. https://doi.org/10.1126/sciadv.1601314

[4] Chakrabarty, A., Healey, E., Shi, D., Zavitsanou, S., Doyle, F. J., & Dassau, E. (2020). Embedded model predictive control for a wearable artificial pancreas. *IEEE Transactions on Control Systems Technology*, *28*(6), 2600–2607. https://doi.org/10.1109/TCST.2019.2939122

[5] Rind, S., Zhang, N., Khan, W. U., & Zhang, Q. (2025). Sweat-based wearable biosensors: A new era of continuous, noninvasive health monitoring and diagnostics. *Wearable Electronics*, *2*, 323–343. https://doi.org/10.1016/j.wees.2025.08.002

[6] Ji, W., Zhu, J., Wu, W., Wang, N., Wang, J., Wu, J., . . . , & Huo, F. (2021). Wearable sweat biosensors refresh personalized health/medical diagnostics. *Research, 2021*, 9757126. https://doi.org/10.34133/2021/9757126

[7] Sedighi, A., Kou, T., Huang, H., & Li, Y. (2026). Non-invasive on-skin biosensors for monitoring diabetes mellitus. *Nano-Micro Letters*, *18*(1), 16. https://doi.org/10.1007/s40820-025-01843-9

[8] Xiao, J., Liu, Y., Su, L., Zhao, D., Zhao, L., & Zhang, X. (2019). Microfluidic chip-based wearable colorimetric sensor for simple and facile detection of sweat glucose. *Analytical Chemistry*, *91*(23), 14803–14807. https://doi.org/10.1021/acs.analchem.9b03110

[9] Das, R., Nag, S., & Banerjee, P. (2023). Electrochemical nanosensors for sensitization of sweat metabolites: From concept mapping to personalized health monitoring. *Molecules*, *28*(3), 1259. https://doi.org/10.3390/molecules28031259

[10] Mei, X., Yang, J., Liu, J., & Li, Y. (2023). Wearable, nanofiber-based microfluidic systems with integrated electrochemical and colorimetric sensing arrays for multiplex sweat analysis. *Chemical Engineering Journal*, *454*, 140248. https://doi.org/10.1016/j.cej.2022.140248

[11] Leng, Y., & Sun, R. (2025). Multifunctional biomedical devices with closed-loop systems for precision therapy. *Advanced Healthcare Materials*, *14*(31), 2500860. https://doi.org/10.1002/adhm.202500860

[12] Lin, R., Jiang, Z., Chi, Y., Xing, L., Long, Z., Xue, X., & Chen, M. (2026). A flexible wireless skin patch for synchronized glucose monitoring and regulation. *Microsystems & Nanoengineering*, *12*(1), 23. https://doi.org/10.1038/s41378-025-01138-4

[13] Kantesaria, R., & Panda, H. S. (2026). A review on AI-based data-driven models for optimization of nanocarriers as drug delivery systems. *ACS Biomaterials Science & Engineering*, *12*(3), 1397–1418. https://doi.org/10.1021/acsbiomaterials.5c01998

[14] van Durme, R., Crevecoeur, G., Dupré, L., & Coene, A. (2021). Model-based optimized steering and focusing of local magnetic particle concentrations for targeted drug delivery. *Drug Delivery*, *28*(1), 63–76. https://doi.org/10.1080/10717544.2020.1853281

[15] Kang, S. L., Hwang, Y. N., Kwon, J. Y., & Kim, S. M. (2022). Effectiveness and safety of a model predictive control (MPC) algorithm for an artificial pancreas system in outpatients with type 1 diabetes (T1D): Systematic review and meta-analysis. *Diabetology & Metabolic Syndrome*, *14*(1), 187. https://doi.org/10.1186/s13098-022-00962-2

[16] Zhang, K., Wang, J., Liu, T., Luo, Y., Loh, X. J., & Chen, X. (2021). Machine learning-reinforced noninvasive biosensors for healthcare. *Advanced Healthcare Materials*, *10*(17), 2100734. https://doi.org/10.1002/adhm.202100734

[17] Ma, J., Yin, S., Wang, X., Zhang, Q., & Liang, M. (2025). Eprobe: A multi-technique, multi-channel wearable potentiostat. *Biosensors and Bioelectronics: X*, *27*, 100686. https://doi.org/10.1016/j.biosx.2025.100686

[18] Wang, Y., Zeng, L., Song, W., & Liu, J. (2022). Influencing factors and drug application of iontophoresis in transdermal drug delivery: An overview of recent progress. *Drug Delivery and Translational Research*, *12*(1), 15–26. https://doi.org/10.1007/s13346-021-00898-6

[19] Marling, C., & Bunescu, R. (2020). The OhioT1DM dataset for blood glucose level prediction: Update 2020. In *CEUR Workshop Proceedings*, *2675*, 71–74.

[20] Wang, X., Dong, Z., Li, W., Xiao, D., Liu, G., Yu, Z., . . . , & Liang, M. (2025). A high-sensitivity continuous glucose sensor using porous 3D cellulose/carbon nanotube network. *Talanta*, *283*, 127201. https://doi.org/10.1016/j.talanta.2024.127201

[21] Wang, Z., Wang, X., Wen, H., He, Z., Guo, Z., Yin, S., . . . , & Liang, M. (2026). Boron carbide nanoskeleton-engineered wearable biosensor for real-time sweat glucose monitoring. *Advanced Healthcare Materials*, *15*(8), e03624. https://doi.org/10.1002/adhm.202503624

[22] Yin, S., Yu, Z., Song, N., Guo, Z., Li, W., Ma, J., . . . , & Liang, M. (2024). A long lifetime and highly sensitive wearable microneedle sensor for the continuous real-time monitoring of glucose in interstitial fluid. *Biosensors and Bioelectronics*, *244*, 115822. https://doi.org/10.1016/j.bios.2023.115822

[23] Sarkisian, S. V., Ishmael, M. K., & Lenzi, T. (2021). Self-aligning mechanism improves comfort and performance with a powered knee exoskeleton. *IEEE Transactions on Neural Systems and Rehabilitation Engineering*, *29*, 629–640. https://doi.org/10.1109/TNSRE.2021.3064463

How to Cite: Ma, J., Yang, S., Yin, S., Wang, X., & Song, N. (2026). A Modular Closed-Loop Wearable Platform for Sweat Extraction, Analysis, and Drug Delivery. *Smart Wearable Technology*. https://doi.org/10.47852/bonviewSWT62029603

Appendix

Table A1
All detection technologies supported

All supported techniques
Cyclic voltammetry (CV)
Linear sweep voltammetry (LSV)
Staircase voltammetry (SCV)
Tafel plot (TAFEL)
Chronoamperometry (CA)
Chronocoulometry (CC)
Differential pulse voltammetry (DPV)
Normal pulse voltammetry (NPV)
Differential normal pulse voltammetry (DNPV)
Square wave voltammetry (SWV)
Amperometric i-t curve (i-t)
Multi-potential steps (STEP)